# Assessment of collagen fiber orientation dispersion in articular cartilage by small-angle X-ray scattering and diffusion tensor imaging: Preliminary results

Sirisha Tadimalla[a,b], Monique C. Tourell[a,b,i], Robert Knott[c], and Konstantin I. Momot[a,b]*

a School of Chemistry, Physics and Mechanical Engineering, Queensland University of Technology (QUT), Brisbane, QLD 4001, Australia

b Institute of Health and Biomedical Innovation, Kelvin Grove, QLD 4125, Australia

c Australian Nuclear Science and Technology Organisation, Private Mail Bag, Kirrawee, NSW 2232, Australia

i Present address: Monique C. Tourell
School of Chemistry and Institute for Life Sciences
University of Southampton
SO17 1BJ
Southampton
United Kingdom
Email: m.c.tourell@soton.ac.uk

*Correspondence to: Konstantin I. Momot
School of Chemistry, Physics and Mechanical Engineering
Queensland University of Technology (QUT)
GPO Box 2434
Brisbane, QLD 4001
Australia
E-mail: k.momot@qut.edu.au

**Keywords:**

small-angle X-ray scattering (SAXS); diffusion tensor imaging (DTI); articular cartilage; collagen fiber dispersion; fractional anisotropy; orientation distribution function

## ABBREVIATIONS AND SYMBOLS

| | |
|---|---|
| DTI: | diffusion tensor imaging |
| SAXS: | small-angle x-ray scattering |
| FA: | fractional anisotropy |
| ROI: | region of interest |
| AC: | articular cartilage |
| PLM: | polarized light microscopy |
| SEM: | scanning electron microscopy |
| MRI: | magnetic resonance imaging |
| DT: | diffusion tensor |
| MC: | Monte Carlo |
| 2D: | two-dimensional |
| PBS: | phosphate buffered saline |
| NMR: | nuclear magnetic resonance |
| δ: | duration of the diffusion gradient |
| Δ: | diffusion time |
| $\lambda_1, \lambda_2, \lambda_3$ | eigenvalues of the diffusion tensor |
| $\bar{\lambda}$ | mean eigenvalue |
| FWHM: | full width at half maximum |
| $q$: | magnitude of the scattering vector |
| $I_F(\emptyset)$,$I_S(\emptyset)$: | azimuthal intensity distributions of equatorial diffraction maxima |
| $\emptyset$: | azimuthal angle |
| $g(\emptyset)$: | fiber orientation distribution |
| ε: | ellipticity, calculated as 1 - ratio of minimum to maximum value of the distribution |
| $\rho$: | Pearson's correlation coefficient |
| CSD: | constrained spherical deconvolution |

## ABSTRACT

Measurements of the orientational dispersion of collagen fibers in articular cartilage were made using diffusion tensor imaging (DTI) and small-angle X-ray scattering (SAXS) on matched bovine articular cartilage samples. Thirteen pairs of samples were excised from bovine knee joints; each pair was taken from neighboring locations in the same bone. One sample from each pair was used for DTI measurements and the other for SAXS measurements. Fractional anisotropy (FA) values were calculated from the DTI data both for the individual imaging voxels and for whole regions of interest (ROI). The FA values were used as a measure of fiber dispersion and compared to the ellipticities of the fiber orientation distributions obtained from SAXS. Neither the spatially-resolved FA values nor whole-ROI FA values showed any correlation with SAXS ellipticities. We attribute the lack of DTI-SAXS correlation to two principal factors: (1) the significant difference in the imaging resolution of the two techniques; and (2) the inherent limitations of both the SAXS data analysis methodology and the diffusion tensor model in the case of multi-modal fiber orientation distributions. We discuss how these factors could be overcome in future work.

# 1 INTRODUCTION

The collagen fiber network in articular cartilage (AC) is typically described in terms of a zonal architecture, comprising three zones. Fibers situated near the articular surface are predominantly oriented parallel to the articular surface and form the superficial zone. Fibers situated near the bone tend to be oriented almost perpendicular to the articular surface, forming the radial zone. There is also a region of transition between these two zones where fibers are oriented randomly and exhibit no predominant alignment (transitional zone) [1,2]. While the zonal architecture has been observed using a range of techniques such as polarized light microscopy (PLM), scanning electron microscopy (SEM) and magnetic resonance imaging (MRI) [3–5], quantitative and non-destructive determination of the *degree of fiber orientation dispersion* about the predomination direction of alignment is not yet possible.

Diffusion tensor imaging (DTI) is an MRI technique that has gained prominence as a means of studying the local microstructural anisotropy of articular cartilage [6–11]. DTI involves the acquisition of several diffusion-weighted images using diffusion gradients applied in several different directions. The magnetic resonance signal is then least-squares fitted with the model of a diffusion tensor (DT), which can be visualized as an ellipsoid. It is assumed that the characteristics of the diffusion ellipsoid directly reflect the macromolecular environment of the diffusing water molecules [12,13]. Proteoglycans and collagen form most of the macromolecular scaffold of AC [1]. While both these macromolecules restrict the diffusion of water, the diffusion anisotropy in AC is attributed exclusively to the collagen fiber network [8,14].

DTI has been used to observe the changes in the AC collagen fiber network under mechanical loading [15], to characterize tissue degeneration [10,14], and to study collagen fiber anisotropy and tissue microstructure [6,8]. Typically, two parameters are used to describe the collagen fiber network – the direction of the principal eigenvector and the fractional anisotropy (FA) of the DT. AC zonal heights calculated from the principal eigenvectors of the DT were found to be strongly correlated with zonal heights derived from SEM [16]. Spatially-resolved maps of the direction of the principal eigenvector of the DT have also been shown to be consistent with collagen fiber orientation patterns measured by PLM [6], thus establishing the relationship between the principal eigenvector of the DT and the predominant direction of collagen fiber alignment in AC. On the other hand, the FA of the DT is a scalar, dimensionless metric that represents directional differences in the amount of restriction imposed by the collagen fiber network on the diffusion of water molecules. It is computed as the ratio of the standard deviation of the DT eigenvalues to the mean-squared of the eigenvalues. When the restriction is greater in one direction than the others, FA is high (with the upper limit of 1 when diffusion is only possible in a single direction). When the restriction is uniform in all directions, FA is low and tends ideally towards 0, but in practice towards the lower limit determined by the noise level. FA is, therefore, a useful indirect measure of the degree of fiber dispersion [13]. Our research group has previously used Monte Carlo (MC) modelling to identify a quantitative relationship between FA and collagen fiber alignment [17–19]. However, to date, there has been no experimental evaluation of FA as a measure of the degree of fiber orientation dispersion.

We have recently used small angle X-ray scattering (SAXS) measurements to quantify the architecture of the collagen fiber network in AC. 2D SAXS measurements of AC present patterns of diffraction maxima that arise from the structure and orientation of collagen fibers. These patterns were processed to quantitatively determine the distribution of fiber orientations in specific AC samples [20]. In this work, we compare for the first time collagen fiber orientation dispersion measured using DTI with fiber orientation distributions obtained from SAXS on matched bovine AC samples.

# 2 METHODS

## 2.1 Sample preparation

Thirteen bovine knee joints were obtained from a local abattoir and frozen 2 hours after slaughter. Thirteen matched pairs of cylindrical cartilage plugs, of diameter 1 cm, were excised with an intact layer of subchondral bone. The cartilage pairs were obtained from the same bone within the joint and spaced close to each other to ensure matching composition and structure. The thickness of the cartilage layer was typically around 1.5 mm. One cartilage sample of each matched pair (Set A; Table 1) was allocated for DTI measurements, while the other (Set B; Table 1) was used for SAXS measurements. Eight ligament samples of the length 20-30 mm were also excised from the joints for the SAXS experiments. The samples were placed in Phosphate buffered saline (PBS) prepared from PBS concentrate sachets (pH 7.4, NaCl 0.138 M, KCl 0.0027 M; Sigma-Aldrich, Castle Hill, NSW, Australia). Protease inhibitors (Sigma-Aldrich, Australia) and 0.5 mg/mL sodium azide, $NaN_3$ (Sigma-Aldrich, Castle Hill, NSW, Australia) were added to the PBS in order to inhibit metalloproteinase activity and inhibit bacterial growth, respectively. After 24 hours, the samples were blotted dry and frozen until the measurements.

## 2.2 Diffusion tensor imaging

Each cartilage sample in Set A was thawed in the previously prepared PBS solution to room temperature prior to imaging. MR measurements were performed at room temperature on a Bruker Avance nuclear magnetic resonance (NMR) spectrometer (Bruker BioSpin, Rheinstetten, Germany) with a 7.0 T vertical bore superconducting magnet equipped with a Micro2.5 micro-imaging probe. A 15 mm birdcage RF coil was

used. Apparent diffusion-weighted images were acquired using a single-echo diffusion-weighted spin-echo sequence. The samples were oriented such that the normal to the articular surface made an angle of 55° with the direction of the main magnetic field, to obtain the maximum signal to noise ratio by minimizing attenuation of the signal due to spin-spin relaxation. Six of the thirteen AC samples (Samples A1 to A6; Table 1) were imaged using the following parameters: The imaging slice was 1 mm thick and was oriented perpendicular to the articular surface, with an image matrix size = 200 × 160, field of view = 30 mm × 24 mm, echo time = 17 ms, repetition time = 4000 ms, number of averages = 2. The gradient pulse parameters were: $\delta$ = 2 ms, $\Delta$ = 8 ms. The diffusion tensor was sampled in 10 independent gradient directions with two *b*-values per direction set to 650 and 900 s/mm$^2$. A reference image with no diffusion-weighting was also acquired for each *b*-value. The remaining seven of the thirteen AC samples (Samples A7 to A13; Table 1) were imaged using a different set of imaging parameters as follows: The imaging slice was 0.7 mm thick and was oriented perpendicular to the articular surface, with an image matrix size = 160 × 100, field of view = 24 mm × 15 mm, echo time = 15 ms, repetition time = 3000 ms, number of averages = 4. The gradient pulse parameters were: $\delta$ = 2 ms, $\Delta$ = 7 ms. The diffusion tensor was sampled in 60 independent gradient directions with one *b*-value per direction set to 900 s/mm$^2$. Four reference images with no diffusion-weighting were also acquired. The two sample sets were imaged as part of different projects and therefore used slightly different imaging parameters, which are summarized in Table 2.

The elements of the diffusion tensor were obtained from a linearized least-squares fit of the Stejskal-Tanner diffusion-attenuation equation to the measured signal [21]. The

tensor was reconstructed using Mathematica (Wolfram Research, Champaign, Illinois, USA) code written in-house and based on previously published work [6]. Two cartilage regions of interest (ROI) were manually selected in the diffusion-weighted images as shown in Figure 1 – ROIs A and B divided the cartilage into top and bottom halves. In each ROI, two different sets of diffusion tensors were obtained – (a) Spatially resolved diffusion tensors were calculated for each voxel, and (b) a whole-ROI diffusion tensor was calculated by averaging the diffusion-weighted signal intensities in the entire ROI and then calculating the DT from those intensities. The eigenvalues and eigenvectors of the diffusion tensors were computed. Fractional anisotropy (FA) was calculated from each diffusion tensor as [6]

$$FA = \sqrt{\frac{3}{2}}\sqrt{\frac{(\lambda_1 - \bar{\lambda})^2 + (\lambda_2 - \bar{\lambda})^2 + (\lambda_3 - \bar{\lambda})^2}{{\lambda_1}^2 + {\lambda_2}^2 + {\lambda_3}^2}} \quad (1)$$

where $\lambda_1$, $\lambda_2$, $\lambda_3$ are eigenvalues of the diffusion tensor and $\bar{\lambda} = \frac{\lambda_1+\lambda_2+\lambda_3}{3}$. When diffusion is completely isotropic, FA = 0, and when diffusion is completely anisotropic, FA = 1. Non-zero values of FA in the PBS solution surrounding the AC sample estimate the noise FA and were subtracted from the measured FA to obtain the intrinsic FA in AC [13].

## 2.3 Small angle X-ray scattering

Disks of cartilage were obtained from each AC sample in set B by removing the bone. Samples B4, B5 and B6 were incubated at 37°C in 2 mg/mL trypsin (Sigma-Aldrich, Castle Hill, NSW, Australia) solution for 18 hours to deplete proteoglycans, while the remaining samples were kept hydrated in PBS. Strips of 10 mm × 1 mm were then cut

out from each cartilage sample and each strip was halved parallel to the articular surface to form two thinner sections which approximately represented the transitional zone and the radial zone. These sections will be referred to as the top half and the bottom half respectively. The trypsin-treated cartilage strips could not be separated into the two sections as trypsin treatment causes loss of tissue structural integrity. Strips of 10 mm $\times$ 1 mm were also cut out from all ligament samples using a scalpel. Two ligament samples were treated with trypsin for 18 hours, while the other ligament samples were kept hydrated in PBS. All samples were finally placed in quartz capillary tubes (inner diameter 2.5 mm; Hampton Research, Aliso Viejo, CA, USA). Capillary tubes containing AC samples B1 to B6 and ligament samples L1 to L4 were then sealed with wax, while capillary tubes containing AC samples B7 to B13 and ligament samples L5 to L8 remained unsealed.

Data was collected on a NanoSTAR II SAXS instrument (Bruker AXS, Karlsruhe, Germany). The X-ray source was a copper rotating anode (0.3 mm filament) operating at 45 kV and 110 mA (Cu Kα radiation wavelength λ = 0.15418 nm), fitted with Montel multilayer optics and three pin-hole collimation for point focus geometry (750 µm source; 400 µm; 1000 µm diameter pinholes) [22]. The beam was 1 mm diameter full width at half maximum at the sample position. A VÅNTEC 2D detector (2048 × 2048 pixels; pixel size 68 × 68 $\mu m^2$; Bruker AXS, Karlsruhe, Germany) was located centrally about the beam axis, and a 2.85 mm diameter beam-stop was located immediately in front of the detector. The sample to detector distance was calibrated using a standard sample (silver behenate powder) and for these experiments was 72.25 cm. The sample tube was mounted on a three position X-Y translation stage and aligned with the X-ray

beam using a sample absorption scan. The sample position was reproducible to better than 0.01 mm. Optics and sample chamber were under vacuum to minimize background due to air scatter.

2D SAXS data was collected for ligament samples L1 to L8, with the collagen fibers directed predominantly along the length of the capillary and oriented perpendicular to the X-ray beam. Samples L5 to L8 were in unsealed capillary tubes and were dehydrated when placed in the sample chamber for 10 minutes prior to data acquisition. For AC samples B1, B2 and B3, 2D SAXS data for bottom sections were obtained at two orientations with respect to the X-ray beam direction, and the orientation of the top sections with respect to the X-ray beam was unknown. Samples B7 to B13 were placed in unsealed capillary tubes and were dehydrated when placed in the sample chamber for 10 minutes prior to data acquisition. 2D SAXS data for both sections of dehydrated cartilage samples were obtained at two orientations. For cartilage sample B1, SAXS data was acquired in both native and dehydrated states. A summary of the sample preparation and treatment protocol for SAXS experiments is shown in Table 1.

For each sample, 2D SAXS data were collected as a function of scattering vector $q$ over the range $0.15 < q < 3.92$ nm$^{-1}$. Multiple data sets were collected to improve counting statistics. The data sets were averaged to obtain a single data set for analysis. Azimuthal distributions of intensities of meridional diffraction maxima, $I_S^m(\emptyset)$, where $\emptyset$ is the azimuthal angle and "*m*" and "*S*" denote meridional and AC sample respectively, were extracted from the 2D SAXS patterns. Similar azimuthal intensity

distributions of equatorial diffraction maxima, $I_F^e(\emptyset)$ and $I_S^e(\emptyset)$, where "$e$" denotes equatorial and "$F$" denotes ligament sample, were extracted from 2D SAXS patterns of ligament and AC samples respectively. Following previously described methodology [20,23,24], the distribution of fiber orientations, $g(\emptyset)$, in the AC sample and the azimuthal scattering intensity distributions were related as

$$g(\emptyset) = I_S^m(\emptyset) \tag{2}$$

$$I_S^e(\emptyset) = I_F^e(\emptyset) * g(\emptyset) \tag{3}$$

where the superscripts "*m*" and "*e*" refer to the meridional and equatorial scatter, respectively. The collagen fiber orientation distribution in each AC sample was determined as $g(\emptyset)$, which was calculated using Eqs. (2-3). Deconvolution between $I_F^e(\emptyset)$ and $I_S^e(\emptyset)$ was carried out using methodology described previously [20]. Each orientation and section (top or bottom) of the AC samples in Table 1 was treated as an individual sample. Then for each sample, a fiber orientation distribution was obtained from the meridional intensity distribution [see Eq. (2)] and at least two fiber orientation distributions were obtained from the equatorial intensity distribution (by deconvolution with reference ligament samples using Eq. (3)). The number of fiber orientation distributions obtained via deconvolution depended on the number of reference ligament samples available for each AC sample (See Table 1). For example, Figure 2 shows all the fiber orientation distributions (shown as polar plots) calculated for the top half of AC sample B7 from the SAXS pattern obtained at one sample orientation. A quantitative measure of fiber orientation was obtained from each distribution as the ellipticity, defined as

$$\varepsilon = 1 - \frac{min}{max} \quad (4)$$

where $min$ and $max$ are the minimum and maximum values of the distribution, respectively. As demonstrated in our previous work [20], there is no significant difference between fiber orientation distributions calculated from meridional and equatorial diffraction maxima. Therefore, the degree of fiber alignment in each sample was taken as the average of the ellipticities calculated for all fiber orientation distributions obtained for the given AC sample.

# 3 RESULTS

Figure 3 shows a comparison of spatially-resolved FA values obtained from DTI measurements of AC samples in set A versus ellipticities of the fiber orientation distributions obtained from SAXS measurements of matched AC samples in set B. Ellipticities calculated from SAXS patterns obtained at two orientations of the same sample were averaged to obtain a single representative measure of fiber orientation dispersion in the sample. FA values in this figure were calculated as the mean of spatially-resolved FA values obtained from spatially resolved diffusion tensors in each voxel in the cartilage ROI. For samples in set B which were separated into top and bottom sections, FA values were correspondingly calculated from the bottom (ROI A) and top (ROI B) halves. In the figure, data points from the two ROIs are represented by blue squares (bottom halves) and orange circles (top halves). Correlation between spatially-resolved FA and SAXS ellipticities was calculated as the Pearson's correlation coefficient [25], $\rho = -0.38$ (bottom halves) and $\rho = 0.51$ (top halves).

Figure 4 shows a comparison between whole-ROI FA and SAXS ellipticities of the fiber orientation distributions. The whole-ROI FA values were calculated differently from the spatially-resolved FA values shown in Figure 3. A single diffusion tensor was obtained using diffusion-weighted MR signals averaged over the entire cartilage ROI, resulting in whole-ROI FA values for each ROI. Unlike FA, fiber orientation distributions can be combined linearly. Therefore, ellipticities of fiber orientation distributions obtained at all sample orientations with respect to the X-ray beam were averaged to obtain a single ellipticity value that described the fiber orientation distribution in the AC sample. Top and bottom halves of the samples, represented by orange circles and blue

squares respectively, were treated as separate samples. Correlation between the whole-ROI FA and ellipticities was measured as the Pearson's correlation coefficient, $\rho = 0.07$ (bottom halves) and $\rho = 0.05$ (top halves).

# 4 DISCUSSION

The collagen fiber network in articular cartilage is intimately linked to its biomechanical properties [26–31]. Quantitative knowledge of the fiber architecture is, therefore, important for development of realistic biomechanical models [32–34], bioengineering of the tissue [35] and for evaluation of tissue pathology [36]. Non-invasive methods for quantifying fiber architecture are particularly important, as they allow patient-specific or sample-specific studies of tissue structure and function. MRI is both non-destructive and non-invasive and has become an invaluable tool for the study of articular cartilage [37–39]. $T_2$ imaging and DTI, in particular, are MRI techniques that are known to be sensitive to the collagen fiber orientation within the tissue [40,41]. The aim of this study was to evaluate DTI as a technique for quantitative assessment of the collagen fiber network in AC. Application of DTI for the study of local collagen fiber orientation in AC has so far been based on two characteristics of the DT: (1) the principal eigenvector, which reflects the predominant direction of fiber alignment; and (2) fractional anisotropy, which can serve as a semi-quantitative estimate of fiber dispersion [7–9,11,14]. Several studies have examined and established the link between the direction of the principal eigenvector of the DT and the predominant direction of fiber alignment [6,8,15,16]. The relationship between fractional anisotropy (FA) and collagen fiber dispersion, however, remains relatively unexplored.

In this paper, we examined the utility of FA as a measure of collagen fiber orientation dispersion by comparing the FA from DTI measurements with fiber orientation distributions obtained from SAXS measurements. Simulations of the diffusion tensor in

model fiber networks have shown that FA is strongly dependent on both the collagen fiber alignment and collagen volume fraction [17–19]. However, in articular cartilage, the collagen volume fraction exhibits a limited variation across the depth of the tissue [5]. Therefore, we expected to observe a strong correlation between FA of the diffusion tensor and SAXS ellipticities.

The comparison was non-trivial because, unlike DTI, SAXS is not an imaging technique. That is, it does not produce an image of the sample; rather, it produces a single 2D pattern of scattered X-rays which contains information on the internal structure of the sample. In this study, SAXS data was obtained at a significantly lower spatial resolution than the spatial resolution of the diffusion MR images. As a result, comparison of SAXS ellipticities of fiber orientation distributions (obtained from whole AC samples) with spatially-varying FA values obtained from DTI does not provide meaningful information. Figure 3 shows that the X and Y error bars on each data point are of the order of the full range of FA and SAXS values in the dataset, thus completely masking any potential underlying correlation. This limitation was overcome by making the spatial resolution of DTI and SAXS measurements comparable by down-sampling the diffusion-weighted MR images prior to calculation of the diffusion tensor. This produced a single whole-ROI FA value for a ROI similar to that used for SAXS data acquisition. A comparison of the whole-ROI DTI FA values with the SAXS ellipticities is shown in Figure 4. However, irrespective of the spatial resolution, there was no clear correlation between DTI FA values and SAXS ellipticities.

This unexpected result may, in part, be attributed to limitations of the experiment design. In this study, SAXS and DTI experiments were performed on matched pairs of AC samples and not on the same AC sample. Sample matching was achieved by extracting each pair from neighboring locations on the same bone. It is, however, known that AC thickness, composition and microstructure can exhibit significant topographical variations even within the same bone [42–45], resulting in a possible mismatch of the collagen fiber network in the sample pairs. Experimental protocols where the same AC sample is used for the non-destructive DTI measurements, followed by destructive SAXS measurements, would allow a less confounded comparison of DTI and SAXS results. Such an experimental design is, however, subject to a synchronized availability of the MRI scanner and SAXS beam-time. Unfortunately, this was not feasible in the present study.

Additionally, in DTI, the diffusion tensor represents the 3D diffusion environment of water molecules within a voxel, while in SAXS the 2D diffraction pattern is dependent on sample orientation with respect to the incident X-ray beam [20] and only represents a projection of the actual 3D fiber orientation distribution within the sample. In this study, we obtained SAXS patterns of several samples at two orientations with respect to the X-ray beam (see Table 1). However, determination of the true 3D fiber orientation distribution within the sample requires the acquisition of 2D SAXS patterns at several sample orientations. A detailed demonstration of the acquisition of 3D SAXS data from trabecular bone can be found in [46]. Use of 3D fiber orientation distributions derived from DTI and SAXS experiments may provide a better dataset for comparison of the two techniques.

Equally importantly, it is clear from the results of this study that low spatial resolution of the SAXS dataset prevents direct comparison of SAXS ellipticities with spatially-resolved FA values. The obvious advantage of an increased spatial resolution of the SAXS dataset is the potential for voxel-to-voxel comparison of DTI and SAXS measurements. Resolution of SAXS data can be greatly improved by performing SAXS measurements using a synchrotron-based X-ray beam source. Such X-ray sources can produce beams with diameters as small as 250 μm × 150 μm, allowing acquisition of spatially resolved SAXS patterns with resolutions similar to diffusion-weighted MRI [36,47]. In such a set of experiments, knowledge of the orientation of the articular surface with respect to the X-ray beam will further allow direct comparison of the preferred direction of collagen fiber alignment as observed using SAXS and DTI.

The lack of correlation between whole-ROI FA and SAXS ellipticities may also stem from the multimodal nature of fiber orientation distributions in the full ROIs. Due to the distinct depth-wise variation in collagen fiber orientations in AC, the top and bottom sections (ROIs A and B) can comprise of a combination of radial and transitional zones, and superficial and transitional zones, respectively. There is significant variability in zonal thicknesses and fiber arrangements in AC samples [6]; therefore, fiber orientation distributions in both ROI A and ROI B are very likely multimodal. However, the SAXS data processing methodology used in this study assumes a unimodal distribution of fiber orientations within each sample. This assumption was necessary to ensure the stability of the deconvolution method [20]. However, in SAXS datasets obtained at greater spatial resolutions, it is more likely that the distributions will be unimodal, thus justifying the assumption. This will ensure that

fiber orientation distributions derived from the SAXS data closely match the true fiber orientation distributions in the AC samples. This provides a further strong rationale for the use of synchrotron-based SAXS in future studies.

It is also important to note that there is no distinct boundary between the zones in AC. The definition of individual zones is simply a conceptual discretization of the continuous fiber network [48]. Therefore, in some voxels, especially at the supposed boundaries between the zones, it is very likely that the fiber orientation distribution will be multimodal irrespective of the spatial resolution of the DTI and SAXS experiments. This is a source of potential complications, both in terms of the accuracy of sampling the fiber orientation distributions derived from SAXS and the interpretation of FA in terms of collagen fiber dispersion. In such cases, use of only the meridional component of the SAXS pattern, with no need for deconvolution, may allow extraction of the true multimodal fiber orientation distribution. Application of DTI in the case of multimodal fiber orientation distributions, however, would remain erroneous as the diffusion tensor represents an 'average' distribution only, and cannot adequately model multimodal fiber orientation distributions [49–51]. Additionally, while separation of multiple fiber populations within each voxel is neither feasible nor required, extraction of the fiber orientation distribution, whether unimodal or multimodal, instead of a single FA value, may allow a more direct comparison with the fiber orientation distributions derived from SAXS measurements.

Model-free approaches to the processing of diffusion MR images that allow the direct determination of the distribution of collagen fiber orientations in AC are, therefore, of

considerable interest. A promising example is the constrained spherical deconvolution method (CSD), which in the past 10 years has become invaluable in the field of brain fiber tractography, where it is applied to separately identify multiple fiber tracts within an imaging voxel [49,52,53]. The technique allows direct calculation of spatially resolved fiber orientation distributions from diffusion-weighted images obtained at a much greater angular resolution than in conventional DTI, while making no prior assumptions about the nature of the distribution. While hugely successful in brain fiber tractography, CSD has never been applied to diffusion MRI of articular cartilage. Its utility in diffusion MRI of AC, it should be noted, lies not in identification of multiple fiber populations, but simply in the extraction of model-free fiber orientation distributions. Therefore, while significant modification of the deconvolution methodology currently in use in neuroimaging may be needed, extension of the work presented in this paper using CSD analysis and high-resolution SAXS measurements could provide important insights into the potential of diffusion MRI as a non-invasive technique for quantifying the collagen fiber architecture in articular cartilage.

# 5 CONCLUSIONS

In this work, we present a comparative study of DTI and SAXS measurements of the orientational dispersion of collagen fibers in articular cartilage. Fiber dispersion was quantified using the fractional anisotropy of the diffusion tensor and was compared against ellipticities of fiber orientation distributions obtained from SAXS. There was no clear correlation between DTI and SAXS results, indicating the need for greater spatial resolution of SAXS measurements as well as model-free techniques, such as CSD, for analysis of diffusion-weighted MR images of articular cartilage. Despite the lack of correlation between DTI and SAXS measurements of fiber dispersion discussed in this paper, this study is important as it is the first practically demonstrated evaluation of diffusion MRI as a non-invasive tool for quantitative assessment of the collagen fiber architecture in articular cartilage, using direct comparisons of fiber dispersion measurements by DTI and SAXS. The lessons learned from the negative results of the present work will inform the methodology of future SAXS microstructural studies of articular cartilage.


# ACKNOWLEDGEMENTS

We thank Teys Bros (Beenleigh, QLD, Australia) for providing bovine knee joints for the research.

# FUNDING SOURCES

This work was supported by the Australian Institute of Nuclear Science and Engineering [grants ALNGRA14051 and ALNGRA15025] and by the Institute of Health and Biomedical Innovation, Queensland, Australia.

# REFERENCES


[1] Pearle AD, Warren RF, Rodeo SA. Basic science of articular cartilage and osteoarthritis. Clin Sports Med 2005;24:1–12.

[2] Xia Y, Momot KI, Chen Z, Chen CT, Kahn D, Badar F. Introduction to Cartilage. In: Xia Y, Momot K, editors. Biophys. Biochem. Cartil. by NMR MRI, Cambridge, UK: Royal Society of Chemistry; 2016, p. 1–43.

[3] Benninghoff A. Form und bau der Gelenknorpel in ihren Bezeihungen zur Funktion. Forschung 1925;2:783–825.

[4] Jeffery AK, Blunn GW, Archer CW, Bentley G. Three-dimensional collagen architecture in bovine articular cartilage. J Bone Jt Surg 1991;73–B:795–801.

[5] Xia Y. Magic-angle effect in magnetic resonance imaging of articular cartilage: a review. Invest Radiol 2000;35:602–21.

[6] de Visser SK, Bowden JC, Wentrup-Byrne E, Rintoul L, Bostrom T, Pope JM, et al. Anisotropy of collagen fibre alignment in bovine cartilage: comparison of polarised light microscopy and spatially resolved diffusion-tensor measurements. Osteoarthr Cartil 2008;16:689–97.

[7] Filidoro L, Dietrich O, Weber J, Rauch E, Oerther T, Wick M, et al. High-resolution diffusion tensor imaging of human patellar cartilage: Feasibility and preliminary findings. Magn Reson Med 2005;53:993–8.

[8] Meder R, de Visser SK, Bowden JC, Bostrom T, Pope JM. Diffusion tensor imaging of articular cartilage as a measure of tissue microstructure. Osteoarthritis Cartilage 2006;14:875–81.

[9] Raya JG, Horng A, Dietrich O, Krasnokutsky S, Beltran LS, Storey P, et al. Articular cartilage: in vivo diffusion-tensor imaging. Radiology 2012;262:550–9.

[10] Ferizi U, Rossi I, Lee Y, Lendhey M, Teplensky J, Kennedy OD, et al. Diffusion tensor imaging of articular cartilage at 3T correlates with histology and biomechanics in a mechanical injury model. Magn Reson Med 2017;78:69–78.

[11] Raya JG. Techniques and applications of in vivo diffusion imaging of articular cartilage. J Magn Reson Imaging 2015;41:1487–504.

[12] Le Bihan D, Mangin J-F, Poupon C, Clark CA, Pappata S, Molko N, et al. Diffusion tensor imaging: Concepts and applications. J Magn Reson Imaging 2001;13:534–46.

[13] Momot KI, Pope JM, Wellard RM. Digital Processing of Diffusion-Tensor Images of Avascular Tissues. In: Dougherty G, editor. Med. image Process. Tech. Appl., NY: Springer; 2011, p. 341–71.

[14] Deng X, Farley M, Nieminen MT, Gray M, Burstein D. Diffusion tensor imaging of native and degenerated human articular cartilage. Magn Reson Imaging 2007;25:168–71.

[15] de Visser SK, Crawford RW, Pope JM. Structural adaptations in compressed

articular cartilage measured by diffusion tensor imaging. Osteoarthritis Cartilage 2008;16:83–9.

[16] Raya JG, Arnoldi AP, Weber DL, Filidoro L, Dietrich O, Adam-Neumair S, et al. Ultra-high field diffusion tensor imaging of articular cartilage correlated with histology and scanning electron microscopy. Magn Reson Mater Physics, Biol Med 2011;24:247–58.

[17] Momot KI. Diffusion tensor of water in model articular cartilage. Eur Biophys J 2011;40:81–91.

[18] Tourell MC, Powell SK, Momot KI. Diffusion tensor of water in partially aligned fibre networks. J Phys D Appl Phys 2013;46:455401.

[19] Powell SK, Momot KI. Langevin dynamics modeling of the water diffusion tensor in partially aligned collagen networks. Phys Rev E 2012;86:1–13.

[20] Tadimalla S, Tourell MC, Knott R, Momot KI. Quantifying collagen fibre architecture in articular cartilage using small-angle X-ray scattering. Biomed Spectrosc Imaging 2017;6:37–57.

[21] Basser PJ, Jones DK. Diffusion-tensor MRI: theory, experimental design and data analysis - a technical review. NMR Biomed 2002;15:456–67.

[22] Pedersen JS. A flux- and background-optimized version of the NanoSTAR small-angle X-ray scattering camera for solution scattering. J Appl Crystallogr 2004;37:369–80.

[23] Brodsky B, BelBruno KC, Hardt TA, Eikenberry EF. Collagen Fibril Structure in Lamprey. J Mol Biol 1994;243:38–47.

[24] Stribeck N. X-ray scattering of soft matter. Berlin, Heidelberg: Springer Berlin Heidelberg; 2007.

[25] Ranganathan P, Pramesh CS, Aggarwal R. Common pitfalls in statistical analysis: Intention-to-treat versus per-protocol analysis. Perspect Clin Res 2016;7:144–6.

[26] Rieppo J, Hyttinen MM, Halmesmaki E, Ruotsalainen H, Vasara A, Kiviranta I, et al. Changes in spatial collagen content and collagen network architecture in porcine articular cartilage during growth and maturation. Osteoarthr Cartil 2009;17:448–55.

[27] Shirazi R, Shirazi-Adl A, Hurtig M. Role of cartilage collagen fibrils networks in knee joint biomechanics under compression. J Biomech 2008;41:3340–8.

[28] Kiviranta P, Rieppo J, Korhonen RK, Julkunen P, Töyräs J, Jurvelin JS. Collagen network primarily controls Poisson's ratio of bovine articular cartilage in compression. J Orthop Res 2006;24:690–9.

[29] Jurvelin JS, Buschmann MD, Hunziker EB. Mechanical anisotropy of the human knee articular cartilage in compression. Proc Inst Mech Eng Part H J Eng Med 2003;217:215–9.

[30] He B, Wu JP, Chim SM, Xu J, Kirk TB. Microstructural analysis of collagen and elastin fibres in the kangaroo articular cartilage reveals a structural divergence

depending on its local mechanical environment. Osteoarthr Cartil 2013;21:237–45.

[31] Bullough P, Goodfellow J. The Significance Of The Fine Structure Of Articular Cartilage. J Bone Jt Surgery, Br Vol 1968;50–B:852–7.

[32] Ateshian GA, Rajan V, Chahine NO, Canal CE, Hung CT. Modeling the Matrix of Articular Cartilage Using a Continuous Fiber Angular Distribution Predicts Many Observed Phenomena. J Biomech Eng 2009;131:61003.

[33] Pierce DM, Unterberger MJ, Trobin W, Ricken T, Holzapfel GA. A microstructurally based continuum model of cartilage viscoelasticity and permeability incorporating measured statistical fiber orientations. Biomech Model Mechanobiol 2016;15:229–44.

[34] Pierce DM, Ricken T, Holzapfel GA. A hyperelastic biphasic fibre-reinforced model of articular cartilage considering distributed collagen fibre orientations: continuum basis, computational aspects and applications. Comput Methods Biomech Biomed Engin 2012;5842:1–18.

[35] Ye K, Felimban R, Moulton SE, Wallace GG, Bella C Di, Traianedes K, et al. Bioengineering of articular cartilage: past, present and future. Regen Med 2013;8:333–49.

[36] Moger CJ, Barrett R, Bleuet P, Bradley DA, Ellis RE, Green EM, et al. Regional variations of collagen orientation in normal and diseased articular cartilage and subchondral bone determined using small angle X-ray scattering (SAXS). Osteoarthritis Cartilage 2007;15:682–7.

[37] Eckstein F, Adam C, Sittek H, Becker C, Milz S, Schulte E, et al. Non-invasive determination of cartilage thickness throughout joint surfaces using magnetic resonance imaging. J Biomech 1997;30:285–9.

[38] Peterfy CG, Guermazi A, Zaim S, Tirman PFJ, Miaux Y, White D, et al. Whole-organ magnetic resonance imaging score (WORMS) of the knee in osteoarthritis. Osteoarthr Cartil 2004;12:177–90.

[39] Stahl R, Blumenkrantz G, Carbadillo-Gamio J, Zhao S, Munoz T, Graverand-Gastineau MPH, et al. MRI-derived T2 relaxation times and cartilage morphometry of the tibo-femoral joint in subjects with and without osteoarthritis during a 1-year follow-up. Osteoarthr Cartil 2007;15:1225–34.

[40] Tadimalla S, Momot KI. Effect of partial H2O-D2O replacement on the anisotropy of transverse proton spin relaxation in bovine articular cartilage. PLoS One 2014;9:e115288.

[41] Momot KI. Microstructural magnetic resonance imaging of articular cartilage. Biomed Spectrosc Imaging 2012;1:27–37.

[42] Carter DR, Beaupre GS, Wong M, Smith RL, Andriacchi TP, Schurman DJ. The Mechanobiology of Articular Cartilage Development and Degeneration. Clin Orthop Relat Res 2004;427:S69–77.

[43] Hunziker EB, Quinn TM, Häuselmann HJ. Quantitative structural organization of

normal adult human articular cartilage. Osteoarthr Cartil 2002;10:564–72.

[44] Armstrong SJ, Read RA, Price R. Topographical variation within the articular cartilage and subchondral bone of the normal ovine knee joint: a histological approach. Osteoarthr Cartil 1995;3:25–33.

[45] Xia Y, Momot KI. Biophysics and Biochemistry of Cartilage by NMR and MRI. 1st ed. Cambridge, UK: Royal Society of Chemistry; 2016.

[46] Georgiadis M, Guizar-Sicairos M, Zwahlen A, Trüssel AJ, Bunk O, Müller R, et al. 3D scanning SAXS: A novel method for the assessment of bone ultrastructure orientation. Bone 2015;71:42–52.

[47] Yarker YE, Hukinst DWL, Nave C. X-ray diffraction studies of tibial plateau cartilage using synchrotron radiation. Connect Tissue Res 1984;12:337–43.

[48] Xia Y. The Critical Role of High Imaging Resolution in MRI of Cartilage - The MRI Microscope. In: Xia Y, Momot KI, editors. Biophys. Biochem. Cartil. by NMR MRI. 1st ed., Cambridge, UK: Royal Society of Chemistry; 2016, p. 455–70.

[49] Tournier J-D, Mori S, Leemans A. Diffusion tensor imaging and beyond. Magn Reson Med 2011;65:1532–56.

[50] Tuch DS. Q-ball imaging. Magn Reson Med 2004;52:1358–72.

[51] Tourell MC, Powell SK, Momot KI. Quantification of Articular Cartilage Microstructure by the Analysis of the Diffusion Tensor. In: Xia Y, Momot KI, editors. Biophys. Biochem. Cartil. by NMR MRI. 1st ed., Cambridge, UK: The Royal Society of Chemistry; 2016, p. 191–224.

[52] Tournier JD, Calamante F, Gadian DG, Connelly A. Direct estimation of the fiber orientation density function from diffusion-weighted MRI data using spherical deconvolution. Neuroimage 2004;23:1176–85.

[53] Tournier JD, Calamante F, Connelly A. Robust determination of the fibre orientation distribution in diffusion MRI: Non-negativity constrained super-resolved spherical deconvolution. Neuroimage 2007;35:1459–72.

# TABLES

Table 1: A summary of AC samples used in DTI and SAXS experiments

| **DTI** | **SAXS** | | | |
|---|---|---|---|---|
| Sample name | Sample name | Treatment | Sectioned into top (T) and bottom (B) sections | Sample orientations for SAXS measurements |
| A1, B1 | B1 | | | |
| A2 | B2 | Untreated | Yes | 2 B, 1 T |
| A3 | B3 | | | |
| A1, B1 | B1_dehyd | Dehydrated | Yes | 2 B, 1 T |
| A4 | B4 | | | |
| A5 | B5 | Treated with trypsin | No | 2 |
| A6 | B6 | | | |
| A7 | B7 | Dehydrated | Yes | 2 B, 2 T |
| A8 | B8 | Dehydrated | Yes | 2 B, 2 T |
| A9 | B9 | Dehydrated | Yes | 2 B, 2 T |
| A10 | B10 | Dehydrated | Yes | 2 B, 2 T |
| A11 | B11 | Dehydrated | Yes | 2 B, 2 T |
| A12 | B12 | Dehydrated | Yes | 2 B, 2 T |
| A13 | B13 | Dehydrated | Yes | 2 B, 2 T |

Table 2: Imaging parameters used for DTI experiments on AC samples

| **Imaging parameters** | **Sample names** | |
|---|---|---|
| | A1, B1, A2, A3, A4, A5, A6 | A7, A8, A9, A10, A11, A12, A13 |
| **Image matrix size** | 200×160 | 160×100 |
| **Field of view** | 30 mm×24 mm | 24 mm×15 mm |
| **Slice thickness** | 1 mm | 0.7 mm |
| **Echo time** | 17 ms | 15 ms |
| **Repetition time** | 4000 ms | 3000 ms |
| **Gradient pulse parameters** | $\delta$ = 2 ms; $\Delta$ = 8 ms | $\delta$ = 2 ms; $\Delta$ = 7 ms |
| **Number of gradient directions** | 10 | 60 |
| **b-value** | 650 s/mm$^2$ and 900 s/mm$^2$ | 900 s/mm$^2$ |

## FIGURE CAPTIONS

Figure 1. Diffusion-weighted image of sample A1 showing the manually selected cartilage ROIs (top half in orange and bottom half in blue). Each ROI is texturized to show the voxels in the region. A single voxel, shown in black, is highlighted as an example. Note that the voxel size shown is not the actual voxel size. Locations of PBS, Teflon plug and bone within the image are also shown.

Figure 2. Fiber orientation distributions (shown as polar plots) calculated from meridional and equatorial components of the 2D SAXS pattern of an articular cartilage sample. Ellipticities obtained from each distribution are also given.

Figure 3. Spatially-resolved FA values obtained from DTI measurements of AC samples, averaged over the top (ROI A; orange circles) and bottom (ROI B; blue squares) halves of the samples, compared with ellipticities of fiber orientation distributions (ε) measured from SAXS experiments on matched AC samples. This plot does not include data from trypsin-treated samples.

Figure 4. Whole-ROI FA values in the top (ROI A; orange circles) and bottom (ROI B; blue squares) halves of the AC samples compared with corresponding SAXS ellipticities (ε) in matched AC samples.

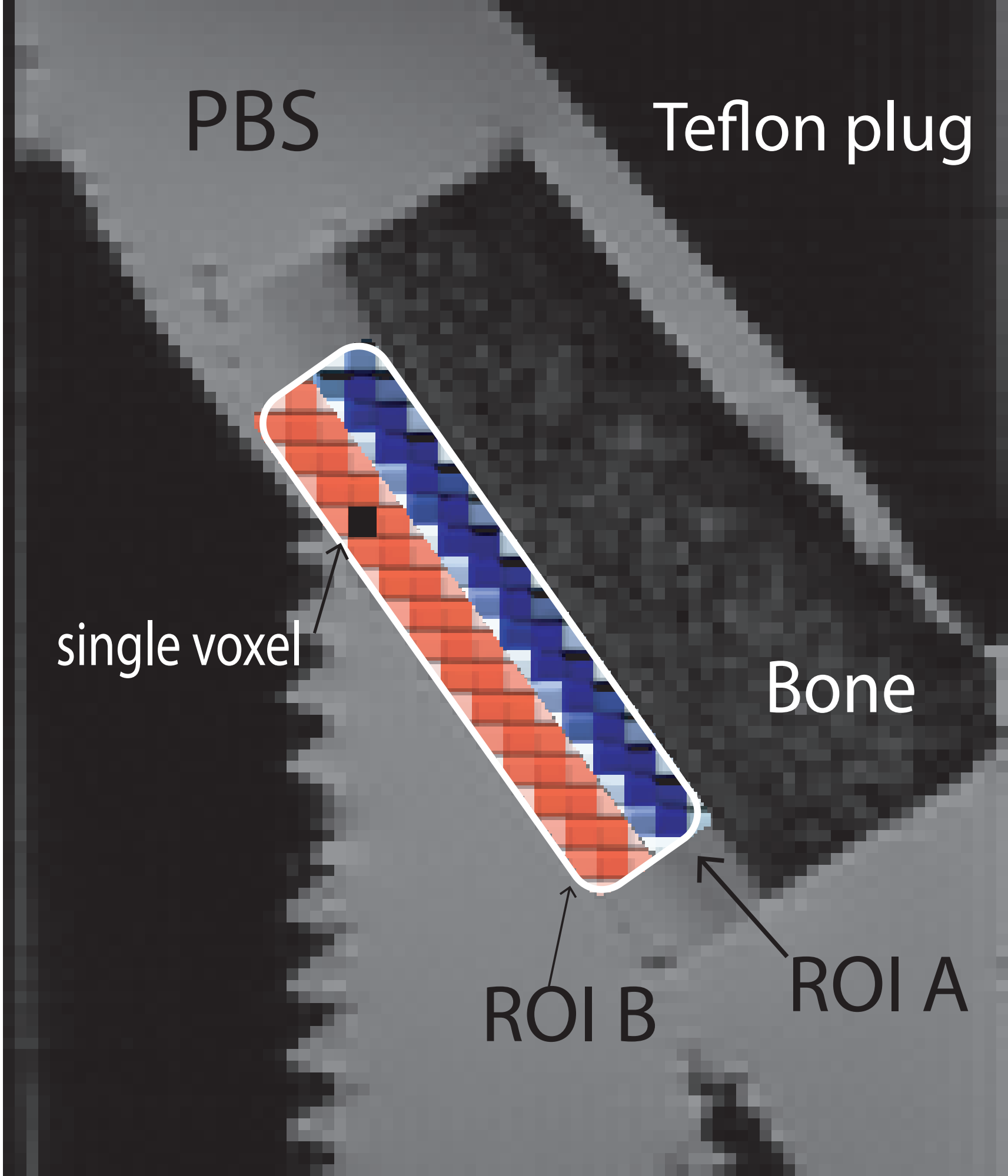
PBS
Teflon plug
single voxel
Bone
ROI B
ROI A

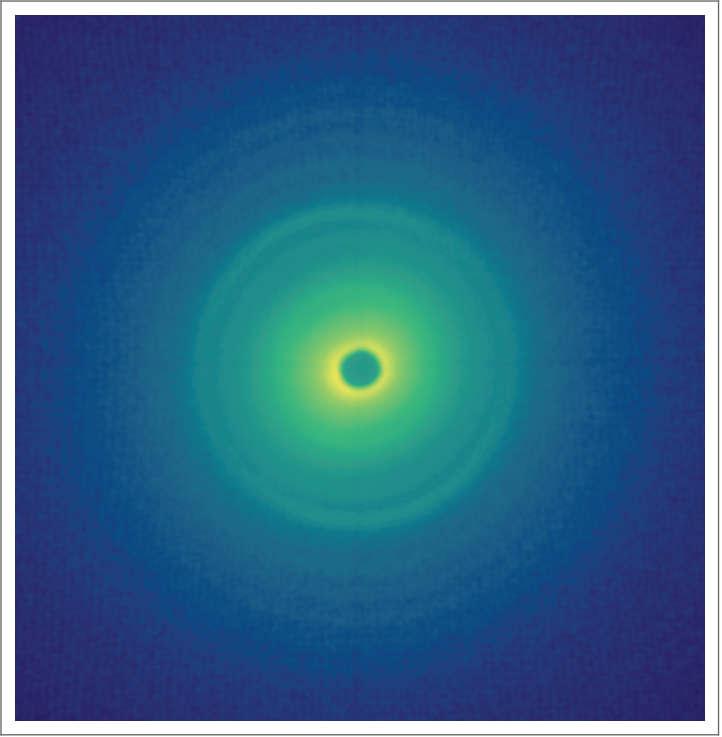

$g(\phi) = I_S^m(\phi)$

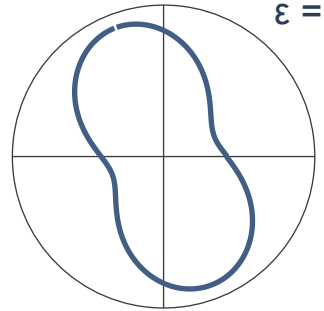


$g(\phi) = deconvolution$
$(I_S^e(\phi), I_F^e(\phi))$

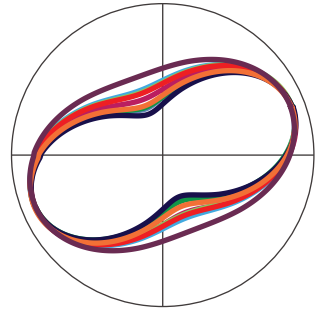

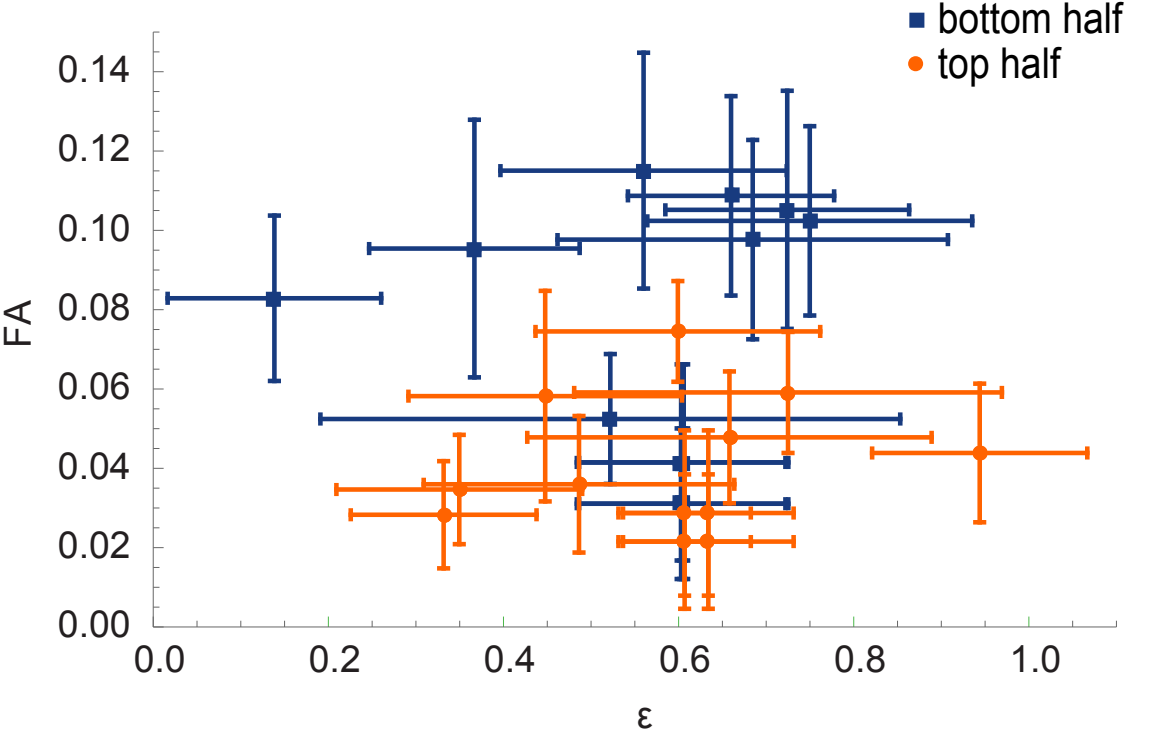
bottom half
top half
FA
0.14
0.12
0.10
0.08
0.06
0.04
0.02
0.00
0.0
0.2
0.4
0.6
0.8
1.0
ε

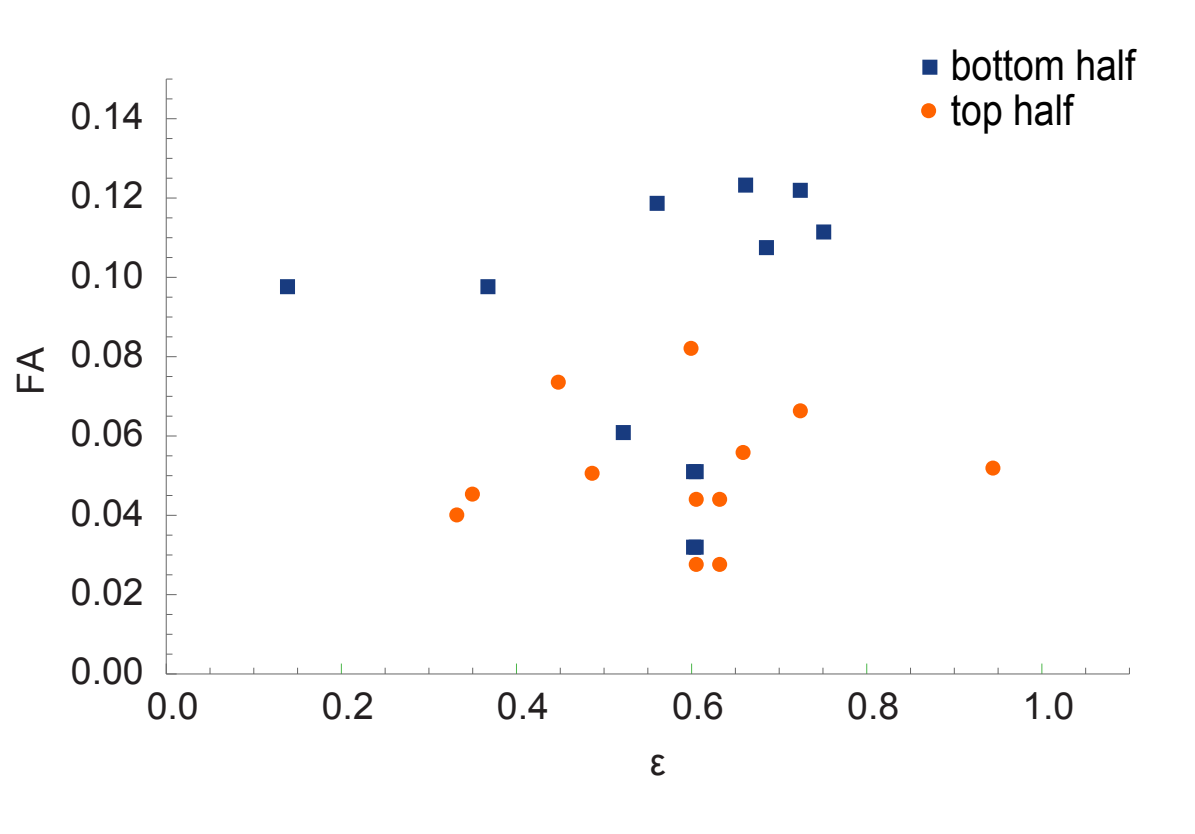
bottom half
top half
0.14
0.12
0.10
0.08
0.06
0.04
0.02
0.00
FA
0.0
0.2
0.4
0.6
0.8
1.0
ε